ACS Photonics

pubs.acs.org/journal/apchd5

Article

Multiphoton Photoluminescence in Hybrid Plasmon–Fiber Cavities with Au and Au@Pd Nanobipyramids: Two-Photon versus Four-Photon Processes and Rapid Quenching

Qi Ai,* Han Zhang, Jianfang Wang, and Harald Giessen*

Cite This: *ACS Photonics* 2021, 8, 2088–2094

Read Online

ACCESS | Metrics & More | Article Recommendations | Supporting Information

ABSTRACT: We investigate the multiphoton photoluminescence (MPPL) characteristics of bare and palladium-capped gold nanobipyramid particles deposited on microfibers with diameters around 1.7 μm. A broad luminescence emission with two evident peaks is detected when the coupled gold nanobipyramid particles are illuminated with a femtosecond laser. By employing multiple peak Lorentz fitting to each PL emission spectrum and performing nonlinear order analysis of the excitation power-dependent measurement, we come to the conclusion that four-photon photoluminescence (4PPL) at around 520 nm and two-photon photoluminescence (2PPL) at longer wavelengths are the main constituents of the broad luminescence emission. Additionally, we observed unexpectedly that those two emission processes have different polarization characteristics. These characteristics can be understood and explained by taking into account the band and crystalline structure of the gold nanobipyramids. Furthermore, the L-band-related 4PPL emission is quenched for Au@Pd nanobipyramids due to the fast transfer of electrons from the gold to the palladium. This provides us with a new way of modifying the photoluminescence in coupled hybrid bimetallic nanostructures. This deeper understanding of MPPL in gold nanoparticles paves the way to precise control of the luminescence emission from plasmonic nanoparticles, which is crucial for further applications in biological imaging and photothermal therapy.

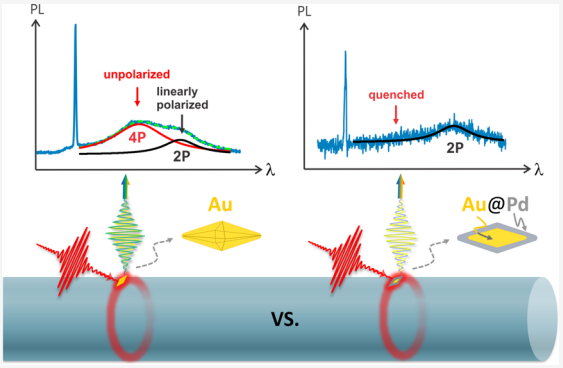

KEYWORDS: *nonlinear plasmonics, multiphoton photoluminescence, nano-optics, gold nanobipyramids, photoluminescence quenching*

Metal nanoantennas have been extensively investigated not only in the linear, but also in the nonlinear optical regime when interacting with femtosecond laser pulses.[1−5] Recently, nonlinear photoluminescence,[6,7] especially two-photon photoluminescence[8−10] of noble metallic nanostructures, is attracting increasing attention because of existent and potential applications in the areas of theranostic biomarkers,[11] bioimaging,[12] and so on. Multiphoton-induced luminescence from noble metals and its enhancement on roughened surfaces have first been reported in the pioneering experiments of Boyd in 1986.[13] Thereafter, gold nanoparticles became one of the most promising photostable and nonblinking single optical biomarkers due to their large extinction cross sections, while the two-photon absorbing process provides the possibility for local heating.[14,15] However, when compared to the investigations about coherent nonlinear processes, such as second- and third-harmonic generation, research about MPPL from isolated gold nanoantennas is still quite rare, and some more analysis is necessary to fully understand and utilize this process. It is mainly limited by its low quantum efficiency. Particularly, higher-order photoluminescence requires even larger peak intensities and local fields.

On the other hand, photoluminescence quite often overlaps with the coherent optical response of the nanoantenna systems in nonlinear spectra, for example, in second- or third-harmonic generation processes.[15−17] In our previous research about hybrid plasmon–fiber cavities, we had clearly seen that the second-harmonic generation (SHG) peak is located on top of a broad and pronounced MPPL background in the nonlinear spectrum. In this case, controlling and modifying the PL process is required for applications. A comprehensive knowledge of the MPPL characteristics and full understanding of the mechanisms are the preconditions of the desired precise control. It is already well-known that 2PPL can be enhanced by a strong local field.[18−20] Our research will offer strong support for this conclusion. Three-photon absorption from single gold nanoantennas has been reported.[21] 4PPL has been observed

Received: March 29, 2021
Published: July 8, 2021

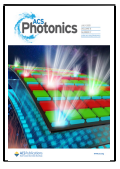

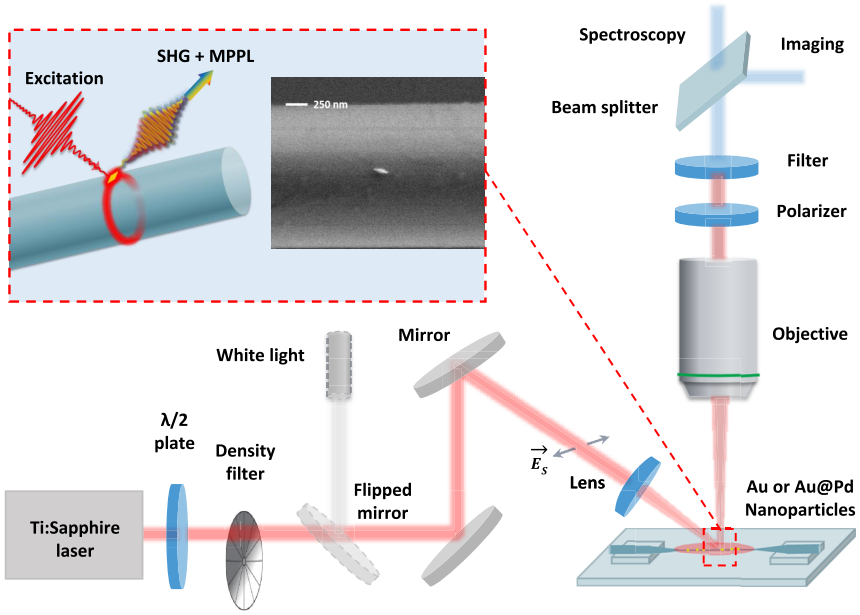

Figure 1. Schematic dark-field setup for white light scattering and nonlinear spectroscopy of single bipyramid nanoparticles on tapered fibers. The schematic diagram and SEM image of the coupling system between an isolated Au nanobipyramid particle and an optical microfiber are shown in the red dashed frame. The incident light is s-pol.

from resonant gold dipole antennas.[22] The dynamics of MPPL has been investigated in gold nanostructures.[6,23] The two- and multiphoton photoluminescence in gold nanoparticles with different shapes and sizes have also been described in numerous publications.[24−28] However, there is still no clear idea on how to modify them in a controlled manner. In addition, knowledge of the spectral and polarization characteristics of MPPL is essential for the control of plasmonic properties.

In our work, we study the photoluminescence from single Au and Pd-capped Au nanobipyramids (NBPs) coupled to silica microfibers. Ultranarrow and enhanced second-harmonic resonances from a similar coupling system have already been reported in our previous paper.[29] By confining more energy in the microfiber cavities, strong interaction over some extended cavity lifetimes between gold nanoparticles and light is achieved. Such an enhanced interaction leads to an orders of magnitude increase of the nonlinear emission. A schematic of this process is presented in the red dashed frame on the left side in Figure 1. An extremely high SHG yield and a broad photoluminescence background with two evident peaks are observed in this plasmon−microfiber hybrid system. By applying multiple-peak Lorentz fitting to the photoluminescence spectra, we clearly find the MPPL in our system to be 2PPL and 4PPL based on the nonlinear order analysis of the excitation power-dependent measurement. Compared to the spectrally resolved nonlinear order analysis, it is more precise to determine the MPPL process. Interestingly, we observe that those two processes have different polarization characteristics. Based on the band and crystalline structures, we give a proper explanation for that, which is very important for designing the proper nanoantenna structures with modified PL processes. The different orientations of gold NBPs deposited on the microfiber induces different peak intensities of linear scattering due to the different coupling strengths. Naturally, a 2PPL with different levels of enhancement effect can be expected. Moreover, the quenching effect of 4PPL is successfully realized by fiber-coupled gold core and palladium shell bipyramid nanostructures. This process is supposed to take place when the electron transfer from gold to palladium takes place.

RESULTS AND DISCUSSION

For the experiment, single-crystalline gold nanobipyramids were synthesized using an optimized seed-mediated method starting with a thermal treatment of common seeds. Compared to conventional seeded growth approaches, those seeds can be stored longer and are more stable for synthesizing bimetallic structures, for example, Au@Pd NBPs investigated in the later experiment.[30] The Au@Pd NBPs were prepared according to a previous report with slight modifications.[31] Process details are described in the Supporting Information. By modifying the aspect ratio of the gold NBPs and the thickness of the palladium in the Au@Pd NBPs, we are able to control their localized plasmon resonances in aqueous solution to be in the same wavelength range centered at around 900 nm (see the ultraviolet (UV)−visible (VIS) spectrum in Figure S1c of the Supporting Information). Representative transmission electron microscopy images (Figure S1b,c) confirm the high uniformity of the gold NBPs and homogeneous palladium shell coating in the bimetallic structures. As the optical cavity of coupled systems, microfibers were fabricated by tapering single mode fibers with a homemade flame-heated pulling machine. We could precisely control the diameter and the waist length of the tapered fiber.[32] In order to achieve the best coupling performance within the working wavelength range of our laser, we designed and pulled microfibers with diameters of around 1.7 μm. The coupled systems were prepared by drop-coating the diluted sample solution onto the hanging tapered fiber surface and waiting for them to dry in ambient air or on the hot plate. The scanning electron microscope image of an isolated coupled gold NBP deposited on the microfiber surface is shown on the right in the red dashed frame in Figure 1.

The experimental microspectroscopy setup is schematically depicted in Figure 1. With a flipped mirror shown as the

https://doi.org/10.1021/acsphotonics.1c00470
ACS Photonics 2021, 8, 2088−2094

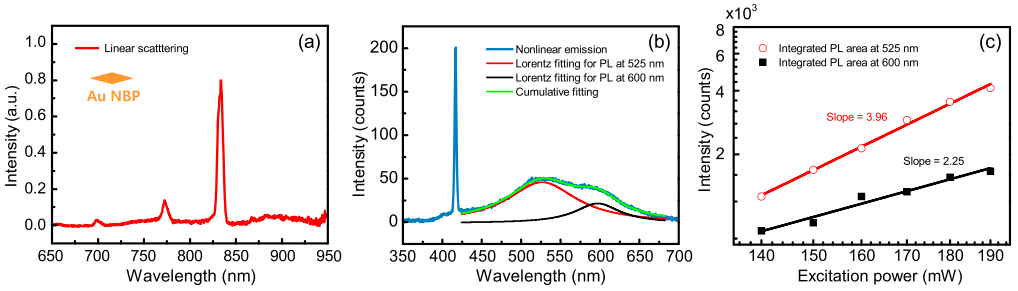

Figure 2. (a) Measured scattering and (b) nonlinear emission spectra of a single gold nanobipyramid particle on a tapered fiber surface. The red and black curves in (b) show the results of multiple (two) peaks Lorentz fitting for the broad PL emission spectra (blue curve) in the range from 425 to 600 nm. The cumulative fitting result (light green curve) excellently fits the measurement spectrum. (c) Integrated intensity of multiphoton photoluminescence centered at 525 and 600 nm in dependence of the excitation power. Excellent linear fitting at log−log scale shows the anticipated power law of the nonlinear responses.

dashed profile, the linear and nonlinear microspectroscopic measurements can easily be realized by switching between a strong incoherent white light source (Energetiq LDLS EQ-99) and a mode-locked Ti:sapphire laser. In order to filter out the scattered light from the microfiber surface, a side-illumination method is utilized. The same incident angle is kept for the linear and nonlinear measurement at all times. Afterward, the samples are imaged by a Nikon LV100 upright microscope and analyzed spectroscopically by a grating spectrometer (Princeton Instruments IsoPlane 160) and a 2D CCD detector (Princeton Instruments PIXIS 256). In the nonlinear measurement, the laser offers a wavelength tuning range of 760−850 nm with a pulse duration of around 100 fs at a repetition rate of 80 MHz. Considering the random orientation of the nanoparticles deposited on the fiber, a half-wave plate is used to ensure the illumination light is s-polarized (parallel to the lab table). In this way, the plasmonic resonance of all the nanoparticles except the one perfectly deposited parallel with the axial direction of the fiber can be excited. The laser is shone onto the sample through a lens with 75 mm focus length at a typical average power of 150 mW. All the samples in our experiment are confirmed to be undamaged by comparing the scattering spectrum before and after the nonlinear measurement. A short-pass filter (FGB37) is placed in the front of the detector to filter out the resonantly scattered laser light.

Figure 2a,b depicts the linear and nonlinear scattering spectra of an isolated gold NBP on the tapered fiber surface. A narrow single band linear resonance is observed due to the efficient coupling between the plasmon mode and one of the cavity modes. Some small peaks near the main resonance are also observed. They are caused by the coupling of the plasmon mode to other cavity modes that are resonant at the edge or out of the plasmon resonance wavelength range.[29] In nonlinear emission spectra, besides the narrow second harmonic peak, two peaks on the broad luminescence background can clearly be seen in the nonlinear spectrum. Considering these two distinguished peaks showing up, a representative multiple peak Lorentz fitting for the luminescence background in the wavelength range between 425 and 680 nm is depicted as a green curve (cumulative fitting) in Figure 2b. It shows an excellent match with the measurement result. In addition, two spectra centered at 525 and 600 nm generated from the fitting results are shown as red and black curves in Figure 2b. They could be considered arising from two different PL processes. In order to determine which PL process takes place at what spectral position, we measured and recorded a series of nonlinear emission spectra excited with laser powers from 140 to 190 mW. Meanwhile, in this measurement, the incident laser wavelength is fixed at 830 nm to match the linear resonance of the coupled system. After applying the multipeak Lorentz fitting to all the measured nonlinear emission spectra above in the same wavelength range, we are able to plot integrated intensities of these two peaks as a function of the excitation power on a double logarithmic scale. The results are displayed in Figure 2c as red open circles and black squares, while the linear fittings for them are depicted as red and black lines. The slope of fitting lines gives the nonlinear order, namely, 2.25 for the PL centered at 600 nm and 3.96 for that at 525 nm. Therefore, we can conclude that the PL process at shorter wavelengths range is mainly dominated by 4PPL, while that one at longer wavelengths range is mainly 2PPL.

Compared to the method used in our former research[29] and some other studies,[7] in particular, spectrally resolved analysis of the nonlinear order, our analysis combined with the multiple peak Lorentz fitting is appropriate for the case of two PL peaks arises in the nonlinear response spectra. It provides us with the most precise information about the nonlinear PL process. Considering the multipeak Lorentz fitting is carried out in the wavelength range from 425 to 680 nm to exclude the SHG effect, the nonlinear order is possibly influenced somehow by the missing part in the shorter wavelength range. In addition, there might be a competition between the 2-photon and 4-photon processes to make a bigger value than 2 for the PL centered at 600 nm.

In order to investigate the polarization characteristics of the PL emission, a polarizer is placed in front of the spectrometer and utilized to perform the emission polarization analysis. As mentioned before, considering the side illumination and the random orientation of the gold NBPs on the fiber surface, the excitation polarization parallel to the optical table is generated and rotated by a half-wave plate. Figure 3 indicates the dependence of the nonlinear emission intensity on the polarizations of the emitted photons. Unexpectedly, the polarization characteristics of the PL centered at about 525 and 600 nm turn out to be different. In the case of the mixed two PL processes, multiple peak Lorentz fitting is still essential for the precise analysis of polarization characteristics. The inset figure in Figure 3a is a typical fitted result. The upper figure inside indicates the angle θ of the polarizer related to the long axis of fiber. After the multiple peak Lorentz fitting is applied to all the θ-dependent nonlinear emission spectra in the wavelength range from 425 to 680 nm, the polar plots of the intensity of fitted PL integrated area as a function of angle θ are displayed in Figure 3b. It proves unambiguously that the

https://doi.org/10.1021/acsphotonics.1c00470
ACS Photonics 2021, 8, 2088−2094

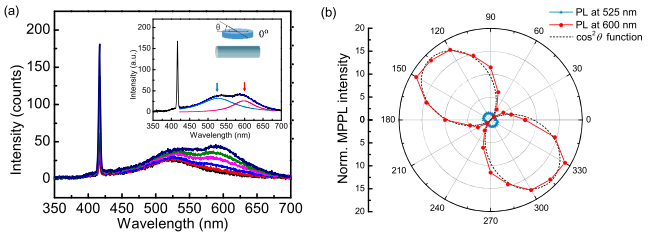

Figure 3. Polarization characteristics of the MPPL from the coupled fiber-gold bipyramid system. (a) Measured nonlinear polarized emission spectra. Inset figure shows the typical multiple peak Lorenz fitting for one nonlinear emission spectrum in the range from 425 to 680 nm. (b) Polar plots of the fitted PL area centered at 525 nm (blue curve) and 600 nm (red curve) as a function of angle θ. The dashed black curve shows a $\cos^2\theta$ function that is characteristic for linearly polarized dipolar emission.

4PPL centered at 525 nm (blue triangles) exhibits definite random polarization, while the 2PPL centered at 600 nm (red dots) shows an almost perfect linear polarization along a certain direction, which is the same as that of the linear scattering emission (Figure S2). This direction is supposed to be along the long axis of the gold NBP. The black dashed line in Figure 3b is a theoretical linearly polarized dipolar-emission generated from a $\cos^2\theta$ function. It perfectly matches with our measurement results.

The origin of the broadband luminescence from plasmonic metals, which is not related to interband radiative recombination, has also been discussed.[33−35] In those investigations, rough disordered noble-metal nanoparticle films or continuous-wave lasers with low power densities are utilized which are not able to excite efficient MPPL. In contrast, high nonlinearity of our hybrid system is confirmed by the excitation power-dependent analyses as depicted in Figure 2. Moreover, the 2PPL process in gold nanostructures excited by short pulse laser sources with strong intensities, which are similar to our excitation conditions, has been experimentally demonstrated to be the result of the radiative recombination of the *d* holes.[10,36] Combined together with several representative studies about the MPPL, we obtain a complete and convincing scheme of the MPPL process in our coupled gold NBP system as illustrated in Figure 4a. It is well-known that in gold crystals optical transitions preferentially occur near the X and L symmetry points in the first Brillouin zone, where the density of states is high. Figure 4a illustrates the band structures mainly including the sp-conduction band and d-band near the X and L symmetry points. According to the calculated band structure, the band gap energy between the d-band and the Fermi surface near the X and L symmetry points are about 1.9 and 2.4 eV, respectively.[37,38] This implies that the peak of PL emission arising from the electron−hole recombination between sp- and d-bands should be observed at around wavelengths of 652 and 517 nm. The spectral peak position at shorter wavelengths observed in Figures 2a and 3a shows perfect agreement with this expectation, while another peak at longer wavelength appears blue-shifted compared to the above calculated result. The main reason is that we use the short-pass filter before the spectrometer, which rejects the signal longer than 600 nm. In this case, it turns out to be difficult to reveal a certain peak position. Meanwhile, the intensity of 2PPL can vary in different fiber-coupled Au NBPs, since 2PPL is strongly enhanced by the linear electron oscillation. We will discuss this enhancement effect later. In Figure 2c, we already determined those two PL processes to rise with powers around 2 and 4, corresponding to the peaks at around 600 and 520 nm. Based on it, we conclude that the 2PPL mainly occurs near the X symmetry point and 4PPL preferentially occurs near the L symmetry point. This observation of 4PPL near the L

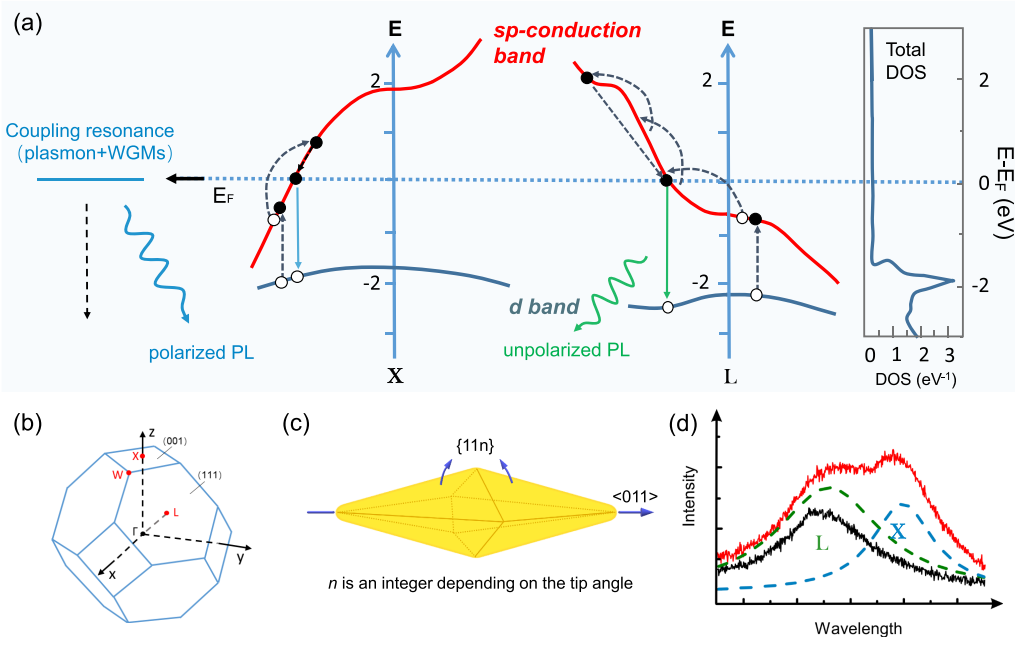

Figure 4. (a) Sketch of the MPPL process within the gold band structure near the X and L symmetry point (2PPL near the X symmetry point and 4PPL near the L symmetry point). The density of states of gold is depicted (right) based on ref 41. (b) Symmetry points in the first Brillouin zone of gold. (c) Schematic structure of the gold nanobipyramid. (d) Measured polarized MPPL spectra (red curve: θ=135°, black curve: θ=45°). Green and blue dashed lines are generated from the two peaks through the Lorentz fitting of the red curve. They correspond to the two processes illustrated in (a) near the X and L symmetry points, respectively.

https://doi.org/10.1021/acsphotonics.1c00470
ACS Photonics 2021, 8, 2088−2094

symmetry point provides a solid confirmation of the temporal dynamics measurement results in resonant nanoantennas as investigated in ref 6. Namely, near the L symmetry point, 4PPL takes place instead of 2PPL when the pulse duration of the excitation laser shortens from >700 to 100 fs. The 2PPL process near the X symmetry point in gold crystals has been widely investigated.[19,26,39] There is a consistent model that 2PPL is the result of two sequential one-photon absorption steps. In detail, the sp-hole is first created by the first photon. Then the second photon excites an electron from the d-band to recombine with the sp-hole in the conduction band. Afterward, the hole in the d-band radiatively recombines with the electron from the conduction band, generating the emitted photon. Similar to 2PPL, 4PPL is triggered by sequential steps of photon absorption. Differently, three intraband transitions within the sp-conduction band occur in the first step. In fact, the multiphoton transition process can also result from sp-direct interband transitions, as illustrated in ref 6. Since a cascade of indirect absorption events is unlikely, direct interband transitions are believed to occur more likely. From our view, both processes are possible. The large near-field localization in our hybrid system can result in an increase of higher-order transition moments. In this case, even symmetry rules no longer prohibit intraband transitions. Thus, we just present one of the proposed processes of three-photon transitions in the sp-band in Figure 4a in order to specify the exact MPPL process at different symmetry points.

Thus, the following question remains: What causes the big difference in the polarization characteristics of the emitted photons between the 2PPL and the 4PPL in our coupled system? We base our explanation on the band and crystal structure of isolated gold NBPs. The gold NBPs are chemically synthesized and thus single crystalline. As shown in Figure 4b,c, the gold NBP is growing along the direction [011]. The side facets are {11n}, where n is an integer depending on the tip angle. The allowed transitions of the recombination emission in the X and L regions follow atomic-dipole selection rules. They are restricted to certain directions.[40] In detail, the direction of transition moment in the X region must be parallel to the xy, yz, or xz planes. Directions of x, y, and z are defined in Figure 4b. In other words, it can be parallel to the long axis of the gold NBPs. The observed emitted photons in the X region are perfectly linearly polarized along the same polarized direction as the linear scattering emission. It is reasonable to suppose that it is caused by the electronic oscillation in the fiber-coupled gold NBP resonantly coupling strongly to the PL as depicted in Figure 4a (left part with the polarized PL emission). On the other hand, the transition moment in the L region only can take the direction parallel to the (111) planes. In the case of the facets of the gold NBP, the (111) plane is not parallel to any axis of the particle. It means the electric vectors of the emitted photons cannot be parallel to the long axis of the gold NBP. As a result, the PL from the L region is almost randomly polarized. Figure 4d illustrates this observation briefly. The red and black curves are the PL emission at $\theta \sim 45°$ and 135°, respectively. The green and blue dashed lines indicate two PL processes generated from the multiple peak Lorentz fitting for the red curve. The PL in the X region is strongly enhanced at $\theta \sim 135°$. Meanwhile, the PL in the L region depends on the angle θ quite only slightly. Hence, the polarization characteristics are properly explained by the crystalline structure and the band structure of the gold NBPs. Similar analysis and results about the polarization characteristics has been also described in a different paper.[36]

Benefiting from the clarification of the PL process and our understanding of the polarization characteristics of PL emission in the system, we designed fiber-coupled Au@Pd NBP to realize the control of the PL process. Similar to the fiber-coupled Au NBP, an ultranarrow linear scattering spectrum is achieved by the coupled Au@Pd NBP, as depicted in Figure 5a. Figure 5b depicts the excitation power-dependent

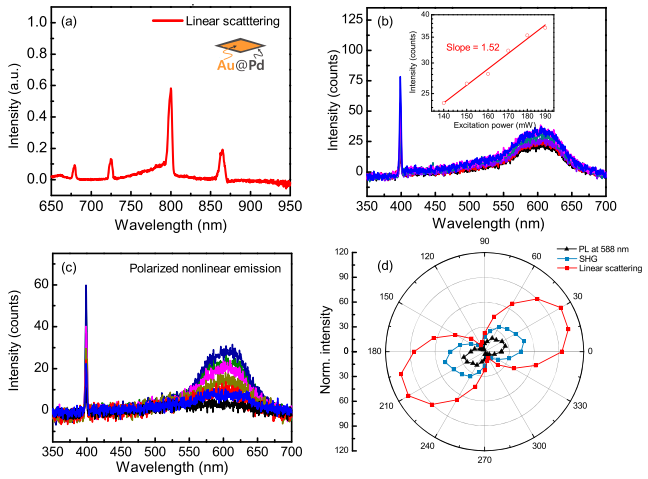

Figure 5. (a) Linear scattering spectrum of a single (gold nanobipyramid core)@(palladium shell) bimetallic nanostructure on the tapered fiber surface. (b) The nonlinear emission spectra excited by different laser powers and the power dependence of integrated PL intensity (inset figure in (b)). (c) Nonlinear emission spectra from the output analyzer with different polarizations. (d) Polar plots of linear scattering, second harmonic generation, and integrated PL intensity as a function of angle θ.

nonlinear emission spectra. Quenching of 4PPL must be present as the second peak at the wavelength around 525 nm is absent. On the other hand, the 2PPL at a longer wavelength is still observed since it is mainly enhanced by the linear electron oscillation. The nonlinear order of 1.52 is determined by the inset figure in Figure 5b. It is worth noting that this result is influenced by the small intensity and the large noise of the PL signal. Figure 5c indicates the dependence of the nonlinear emission intensity on the polarization of the emitted photons. Furthermore, the polar plots of the intensity of linear scattering, SHG, and PL integrated area as a function of angle θ are plotted in Figure 5d. The PL at a longer wavelength is still strongly polarized along the same direction with the linear scattering and SHG. Similar to the coupled gold NBPs, the PL at longer wavelengths can also vary with the different strength of the linear resonance. As shown in Figure S4, a coupled Au@Pd NBP with weaker linear resonance induces a much weaker nonlinear response compared to that one investigated in Figure 5. The 4PPL peak at shorter wavelength is still absent. Meanwhile, a negligible PL peak at longer wavelength is detected. The quenching of PL from the single coupled Au@Pd particle reveals the electron transfer from gold to palladium (see an SEM image of the Au@Pd particles in Figure 6a, where one can nicely see the Pd covering the surface of the gold). The process can be explained reasonably with the band structure of gold and palladium (band structure and density of states for Pd plotted in Figure 6d). We additionally

https://doi.org/10.1021/acsphotonics.1c00470
ACS Photonics 2021, 8, 2088−2094

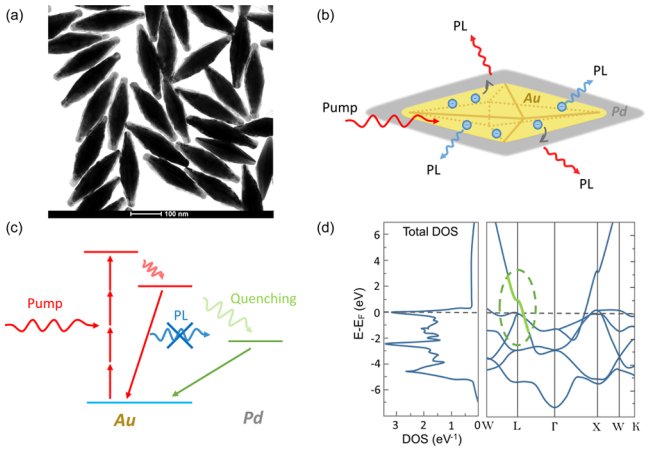

Figure 6. (a) Transmission electron microscope (TEM) image of (gold nanobipyramid core)@(palladium shell) bimetallic nanostructures in aqueous solution. Schematic structure of (b) the electron transfer process in gold@palladium bipyramids and (c) quenching process within the band structure of the gold@palladium bipyramids. (d) Sketch of band structure (right panel) and density of states (left panel) for palladium. Adapted with permission from ref 41. Copyright 2004 American Physical Society.

provide the density of states for Au in the supplement. The d-band in palladium crosses and even exceeds the Fermi surface near the L symmetry point. Meanwhile, the band separation between sp-band and d-band is smaller than that in gold. In this case, palladium provides a high density of states between 0 and 2.5 eV. Thus, the excited electron in the sp-band of gold can transfer easily and fast to palladium before the recombination of electron−hole induces the PL emission. We depict this electron transfer process in Figure 6b. In Figure 6c we indicate in a simplified energy level scheme an intermediate, lower-energy level in Pd, to which the electrons can transfer after being excited in the gold. As a result, the 4PPL is quenched. As we discussed before, the 2PPL is strongly enhanced by the linear electron oscillation. Since the linear resonance of coupled Au@Pd NBPs exhibits the similar linear optical properties as that of coupled Au NBPs, the enhanced 2PPL is still observed in the nonlinear spectra.

In conclusion, a strong nonlinear response, including SHG and MPPL, is achieved by efficient coupling between the plasmon resonance of Au and Au@Pd NBPs and the whispering gallery modes of the tapered fiber. Benefiting from the high nonlinearities of this coupled system, we investigated the higher-order PL properties. Unexpected different polarization characteristics of the two PL processes have been observed. The analysis based on the band and crystalline structure of gold NBPs provides us with a deeper understanding of the MPPL process, demonstrating crystal structure dependence. Moreover, quenching of 4PPL has been detected by coating palladium onto the gold NBPs, which are coupled to the tapered fiber, resulting from fast electron transfer from Au to Pd. This opens a new door to design plasmon nanostructures and then modify the MPPL process in isolated nanoparticles, which is required in potential biotechnology applications.

■ ASSOCIATED CONTENT

Supporting Information

The Supporting Information is available free of charge at https://pubs.acs.org/doi/10.1021/acsphotonics.1c00470.

Preparation and characteristics of the Au and Au@Pd; polarization characteristics of linear scattering and SHG in the fiber-coupled gold NBPs; another coupled gold NBP; another coupled Au@Pd NBP (PDF)

■ AUTHOR INFORMATION

Corresponding Authors

Qi Ai − *4th Physics Institute and Research Center SCoPE, University of Stuttgart, 70569 Stuttgart, Germany;* orcid.org/0000-0002-1716-7638; Email: q.ai@pi4.uni-stuttgart.de

Harald Giessen − *4th Physics Institute and Research Center SCoPE, University of Stuttgart, 70569 Stuttgart, Germany;* Email: h.giessen@pi4.uni-stuttgart.de

Authors

Han Zhang − *Department of Physics, The Chinese University of Hong Kong, Shatin, Hong Kong SAR, China*

Jianfang Wang − *Department of Physics, The Chinese University of Hong Kong, Shatin, Hong Kong SAR, China;* orcid.org/0000-0002-2467-8751

Complete contact information is available at: https://pubs.acs.org/10.1021/acsphotonics.1c00470

Notes

The authors declare no competing financial interest.

■ ACKNOWLEDGMENTS

We would like to thank Deutsche Forschungsgemeinschaft (GRK2642, SPP1839), Bundesministerium für Bildung und Forschung, European Research Council (ERC Advanced Grant ComplexPlas), Ministerium für Forschung und Kunst Baden-Württemberg (IQST), Zeiss Stiftung, and Baden-Württemberg Stiftung for funding. Q.A. acknowledges CSC for funding. We would like to thank Mario Hentschel for taking high-resolution SEM and STEM images and for performing EDX, Ksenia Weber for proofreading and helpful advice, and Florian Sterl for help with the microspectroscopy setup.

■ REFERENCES

(1) Lee, J.; Tymchenko, M.; Argyropoulos, C.; Chen, P. Y.; Lu, F.; Demmerle, F.; Boehm, G.; Amann, M. C.; Alù, A.; Belkin, M. A. Giant Nonlinear Response from Plasmonic Metasurfaces Coupled to Intersubband Transitions. *Nature* **2014**, *511* (7507), 65−69.

(2) Ko, K. D.; Kumar, A.; Fung, K. H.; Ambekar, R.; Liu, G. L.; Fang, N. X.; Toussaint, K. C. Nonlinear Optical Response from Arrays of Au Bowtie Nanoantennas. *Nano Lett.* **2011**, *11* (1), 61−65.

(3) Aouani, H.; Rahmani, M.; Navarro-Cía, M.; Maier, S. A. Third-Harmonic-Upconversion Enhancement from a Single Semiconductor Nanoparticle Coupled to a Plasmonic Antenna. *Nat. Nanotechnol.* **2014**, *9* (4), 290−294.

(4) Celebrano, M.; Wu, X.; Baselli, M.; Großmann, S.; Biagioni, P.; Locatelli, A.; De Angelis, C.; Cerullo, G.; Osellame, R.; Hecht, B.; Duò, L.; Ciccacci, F.; Finazzi, M. Mode Matching in Multiresonant Plasmonic Nanoantennas for Enhanced Second Harmonic Generation. *Nat. Nanotechnol.* **2015**, *10* (5), 412−417.

(5) Gui, L.; Bagheri, S.; Strohfeldt, N.; Hentschel, M.; Zgrabik, C. M.; Metzger, B.; Linnenbank, H.; Hu, E. L.; Giessen, H. Nonlinear Refractory Plasmonics with Titanium Nitride Nanoantennas. *Nano Lett.* **2016**, *16* (9), 5708−5713.

(6) Biagioni, P.; Brida, D.; Huang, J. S.; Kern, J.; Duò, L.; Hecht, B.; Finazzi, M.; Cerullo, G. Dynamics of Four-Photon Photoluminescence in Gold Nanoantennas. *Nano Lett.* **2012**, *12* (6), 2941−2947.

(7) Knittel, V.; Fischer, M. P.; De Roo, T.; Mecking, S.; Leitenstorfer, A.; Brida, D. Nonlinear Photoluminescence Spectrum of Single Gold Nanostructures. *ACS Nano* **2015**, *9* (1), 894−900.
(8) Lien, M. B.; Kim, J. Y.; Han, M. G.; Chang, Y. C.; Chang, Y. C.; Ferguson, H. J.; Zhu, Y.; Herzing, A. A.; Schotland, J. C.; Kotov, N. A.; Norris, T. B. Optical Asymmetry and Nonlinear Light Scattering from Colloidal Gold Nanorods. *ACS Nano* **2017**, *11* (6), 5925−5932.
(9) Imura, K.; Okamoto, H. Properties of Photoluminescence from Single Gold Nanorods Induced by Near-Field Two-Photon Excitation. *J. Phys. Chem. C* **2009**, *113* (27), 11756−11759.
(10) Biagioni, P.; Celebrano, M.; Savoini, M.; Grancini, G.; Brida, D.; Mátéfi-Tempfli, S.; Mátéfi-Tempfli, M.; Duò, L.; Hecht, B.; Cerullo, G.; Finazzi, M. Dependence of the Two-Photon Photoluminescence Yield of Gold Nanostructures on the Laser Pulse Duration. *Phys. Rev. B: Condens. Matter Mater. Phys.* **2009**, *80* (4), 1−5.
(11) Gobin, A. M.; Lee, M. H.; Halas, N. J.; James, W. D.; Drezek, R. A.; West, J. L. Near-Infrared Resonant Nanoshells for Combined Optical Imaging and Photothermal Cancer Therapy. *Nano Lett.* **2007**, *7* (7), 1929−1934.
(12) Wang, S.; Xi, W.; Cai, F.; Zhao, X.; Xu, Z.; Qian, J.; He, S. Three-Photon Luminescence of Gold Nanorods and Its Applications for High Contrast Tissue and Deep in Vivo Brain Imaging. *Theranostics* **2015**, *5* (3), 251−266.
(13) Boyd, G. T.; Yu, Z. H.; Shen, Y. R. Photoinduced Luminescence from the Noble Metals and Its Enhancement on Roughened Surfaces. *Phys. Rev. B: Condens. Matter Mater. Phys.* **1986**, *33* (12), 7923−7936.
(14) Olesiak-Banska, J.; Waszkielewicz, M.; Obstarczyk, P.; Samoc, M. Two-Photon Absorption and Photoluminescence of Colloidal Gold Nanoparticles and Nanoclusters. *Chem. Soc. Rev.* **2019**, *48* (15), 4087−4117.
(15) Durr, N. J.; Larson, T.; Smith, D. K.; Korgel, B. A.; Sokolov, K.; Ben-Yakar, A. Two-Photon Luminescence Imaging of Cancer Cells Using Molecularly Targeted Gold Nanorods. *Nano Lett.* **2007**, *7* (4), 941−945.
(16) Ghenuche, P.; Cherukulappurath, S.; Taminiau, T. H.; Van Hulst, N. F.; Quidant, R. Spectroscopic Mode Mapping of Resonant Plasmon Nanoantennas. *Phys. Rev. Lett.* **2008**, *101* (11), 1−4.
(17) Huang, J. S.; Kern, J.; Geisler, P.; Weinmann, P.; Kamp, M.; Forchel, A.; Biagioni, P.; Hecht, B. Mode Imaging and Selection in Strongly Coupled Nanoantennas. *Nano Lett.* **2010**, *10* (6), 2105−2110.
(18) Melentiev, P. N.; Afanasiev, A. E.; Kuzin, A. A.; Zablotskiy, A. V.; Balykin, V. I. Giant Enhancement of Two Photon Induced Luminescence in Metal Nanostructure. *Opt. Express* **2015**, *23* (9), 11444.
(19) Wackenhut, F.; Wang, X.; Failla, A. V.; Meixner, A. J. Two and Three Photon Excited Luminescence of Single Gold Nanoparticles: Switching between Plasmon- and Electron-Hole-Pair Emission by Ultrashort Laser Pulses. *arXiv:1812.01409 [physics.optics]* **2018**, na.
(20) Beversluis, M.; Bouhelier, A.; Novotny, L. Continuum Generation from Single Gold Nanostructures through Near-Field Mediated Intraband Transitions. *Phys. Rev. B: Condens. Matter Mater. Phys.* **2003**, *68* (11), 1−10.
(21) Farrer, R. A.; Butterfield, F. L.; Chen, V. W.; Fourkas, J. T. Highly Efficient Multiphoton-Absorption-Lnduced Luminescence from Gold Nanoparticles. *Nano Lett.* **2005**, *5* (6), 1139−1142.
(22) Muhlschlegel, P. Resonant Optical Antennas. *Science (Washington, DC, U. S.)* **2005**, *308* (5728), 1607−1609.
(23) Sakat, E.; Bargigia, I.; Celebrano, M.; Cattoni, A.; Collin, S.; Brida, D.; Finazzi, M.; D'Andrea, C.; Biagioni, P. Time-Resolved Photoluminescence in Gold Nanoantennas. *ACS Photonics* **2016**, *3* (8), 1489−1493.
(24) Siddiquee, A. M.; Taylor, A. B.; Syed, S.; Lim, G. H.; Lim, B.; Chon, J. W. M. Measurement of Plasmon-Mediated Two-Photon Luminescence Action Cross Sections of Single Gold Bipyramids, Dumbbells, and Hemispherically Capped Cylindrical Nanorods. *J. Phys. Chem. C* **2015**, *119* (51), 28536−28543.
(25) Gao, N.; Chen, Y.; Li, L.; Guan, Z.; Zhao, T.; Zhou, N.; Yuan, P.; Yao, S. Q.; Xu, Q. H. Shape-Dependent Two-Photon Photoluminescence of Single Gold Nanoparticles. *J. Phys. Chem. C* **2014**, *118* (25), 13904−13911.
(26) Guan, Z.; Gao, N.; Jiang, X. F.; Yuan, P.; Han, F.; Xu, Q. H. Huge Enhancement in Two-Photon Photoluminescence of Au Nanoparticle Clusters Revealed by Single-Particle Spectroscopy. *J. Am. Chem. Soc.* **2013**, *135* (19), 7272−7277.
(27) Deng, H. D.; Li, G. C.; Dai, Q. F.; Ouyang, M.; Lan, S.; Trofimov, V. A.; Lysak, T. M. Size Dependent Competition between Second Harmonic Generation and Two-Photon Luminescence Observed in Gold Nanoparticles. *Nanotechnology* **2013**, *24* (7), 075201.
(28) Sivis, M.; Pazos-Perez, N.; Yu, R.; Alvarez-Puebla, R.; García de Abajo, F. J.; Ropers, C. Continuous-Wave Multiphoton Photoemission from Plasmonic Nanostars. *Commun. Phys.* **2018**, *1* (1), 13.
(29) Ai, Q.; Gui, L.; Paone, D.; Metzger, B.; Mayer, M.; Weber, K.; Fery, A.; Giessen, H. Ultranarrow Second-Harmonic Resonances in Hybrid Plasmon-Fiber Cavities. *Nano Lett.* **2018**, *18* (9), 5576−5582.
(30) Sánchez-Iglesias, A.; Winckelmans, N.; Altantzis, T.; Bals, S.; Grzelczak, M.; Liz-Marzán, L. M. High-Yield Seeded Growth of Monodisperse Pentatwinned Gold Nanoparticles through Thermally Induced Seed Twinning. *J. Am. Chem. Soc.* **2017**, *139* (1), 107−110.
(31) Yip, H. K.; Zhu, X.; Zhuo, X.; Jiang, R.; Yang, Z.; Wang, J. Gold Nanobipyramid-Enhanced Hydrogen Sensing with Plasmon Red Shifts Reaching ≈140 Nm at 2 Vol% Hydrogen Concentration. *Adv. Opt. Mater.* **2017**, *5* (24), 1700740.
(32) Pricking, S.; Giessen, H. Tapering Fibers with Complex Shape. *Opt. Express* **2010**, *18* (4), 3426.
(33) Haug, T.; Klemm, P.; Bange, S.; Lupton, J. M. Hot-Electron Intraband Luminescence from Single Hot Spots in Noble-Metal Nanoparticle Films. *Phys. Rev. Lett.* **2015**, *115* (6), 1−5.
(34) He, Y.; Xia, K.; Lu, G.; Shen, H.; Cheng, Y.; Liu, Y. C.; Shi, K.; Xiao, Y. F.; Gong, Q. Surface Enhanced Anti-Stokes One-Photon Luminescence from Single Gold Nanorods. *Nanoscale* **2015**, *7* (2), 577−582.
(35) Hugall, J. T.; Baumberg, J. J. Demonstrating Photoluminescence from Au Is Electronic Inelastic Light Scattering of a Plasmonic Metal: The Origin of SERS Backgrounds. *Nano Lett.* **2015**, *15* (4), 2600−2604.
(36) Imura, K.; Nagahara, T.; Okamoto, H. Near-Field Two-Photon-Induced Photoluminescence from Single Gold Nanorods and Imaging of Plasmon Modes. *J. Phys. Chem. B* **2005**, *109* (27), 13214−13220.
(37) Rosei, R. Temperature Modulation of the Optical Transitions Involving the Fermi Surface in Ag: Theory. *Phys. Rev. B* **1974**, *10* (2), 474−483.
(38) Guerrisi, M.; Rosei, R.; Winsemius, P. Splitting of the Interband Absorption Edge in Au. *Phys. Rev. B* **1975**, *12* (2), 557−563.
(39) Remesh, V.; Stührenberg, M.; Saemisch, L.; Accanto, N.; Van Hulst, N. F. Phase Control of Plasmon Enhanced Two-Photon Photoluminescence in Resonant Gold Nanoantennas. *Appl. Phys. Lett.* **2018**, *113* (21), 211101.
(40) Bouckaert, L. P.; Smoluchowski, R.; Wigner, E. Theory of Brillouin Zones and Symmetry Properties of Wave Functions in Crystals. *Phys. Rev.* **1936**, *50* (1), 58−67.
(41) Ladstädter, F.; Hohenester, U.; Puschnig, P.; Ambrosch-Draxl, C. First-Principles Calculation of Hot-Electron Scattering in Metals. *Phys. Rev. B: Condens. Matter Mater. Phys.* **2004**, *70* (23), 1−10.

https://doi.org/10.1021/acsphotonics.1c00470
ACS Photonics 2021, 8, 2088−2094